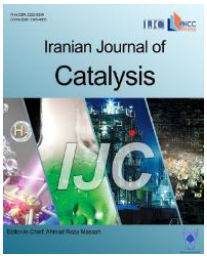

Iran. J. Catal. 2026; 16(1): 61-79

Iranian Journal of Catalysis (IJC)

https://doi.org/10.57647/ijc.2026.1601.05

Research Article

Enhanced Photocatalytic Degradation of Turquoise Blue G (TBG) Dye Using Cu:ZnO/TiO_2 Nanoheterojunction Photocatalyst

Mangesh K. Lanjewar[1,2], Omprakash K. Mahadwad[3,*], Pritam Patil[4]

[1]*Research Scholar, Gujarat Technological University, Ahmedabad, India*
[2]*Department of Chemical Engineering, Government Engineering College, Bharuch, India*
[3]*Department of Chemical Technology, UPL University of Sustainable Technology, Ankleshwar, India*
[4]*Department of Chemical Engineering, Shri S'ad Vidya Mandal Institute of Technology, Bharuch, India*

[*]**Corresponding authors:** omprakash.mahadwad@upluniversity.ac.in

Article History:

Received:
07 July 2025

Revised:
31 October 2025

Accepted:
10 November 2025

Published Online:
25 November 2025

Published in Issue:
31 March 2026

Abstract

Pure TiO_2, ZnO, ZnO/TiO_2, and Cu doped ZnO/TiO_2 (Cu:ZnO/TiO_2) heterojunctions (Type II) photocatalysts were successfully synthesized using a cost-effective room-temperature sol-gel (RTSG) method. Copper (Cu) doping levels ranged from 3 to 9 wt% relative to ZnO. The structural, morphological, optical, and surface chemical properties were characterized using XRD, FESEM, UV–Vis spectroscopy, XPS, and FTIR. Among all samples, 7 wt% Cu:ZnO/TiO_2 exhibited a prominent red shift in the absorption edge (from 388.7 to 413.33 nm) and a narrowed band gap of 3.0 eV compared to 3.19 eV for pure TiO_2, indicating enhanced visible-light absorption. This optimized photocatalyst demonstrated outstanding photocatalytic efficiency for the first-time degradation of Turquoise Blue G (TBG) dye, achieving 95% degradation within 2.5 h under UV irradiation-1.52 times higher than pure TiO_2. The Chemical Oxygen Demand (COD) decreased by 77.78%, confirming effective mineralization. Kinetic analysis revealed that the degradation followed pseudo-first-order kinetics, validating the reaction's rate dependence on dye concentration. The recycled photocatalyst retained 84.3% degradation efficiency and 60% COD reduction, indicating excellent reusability. Furthermore, the highest adsorption capacity was observed at lower pH (pH 4), favoring electrostatic attraction. These results establish 7% Cu:ZnO/TiO_2 as a robust, reusable, and highly efficient photocatalyst for sustainable dye wastewater treatment.

Keywords: Type II heterojunction photocatalyst; Sol-gel method; Turquoise blue G (TBG) dye; Photocatalytic degradation

Cite this article: M. K. Lanjewar, O. K. Mahadwad , P. Patil, Iran. J. Catal. **16** (2026) 61-79. https://doi.org/10.57647/ijc.2026.1601.05

1. Introduction

Among various advanced oxidation processes (AOPs), heterogeneous photocatalytic processes have proven effective in degrading a wide range of pollutants without generating harmful intermediates [1–3]. Numerous industries including textile, pharmaceutical, leather, pesticide, chemical, petrochemical, and paint discharge various organic pollutants into water bodies [1,2,4]. These pollutants are significant threats to aquatic ecosystems and human health, and are highly resistant to natural degradation. Semiconductor metal oxides, particularly

TiO_2 and ZnO, are among the most promising photocatalysts for treating organic contaminants. However, their wide intrinsic band gaps and the rapid recombination of photogenerated charge carriers limit their efficiency under UV-visible light irradiation [5,6]. Many research studies have reported that doping and co-doping of TiO_2 and ZnO with transition metals, noble metals, and non-metals can enhance their photocatalytic activity, thereby improving the degradation of wastewater pollutants [7,8].

Furthermore, both ZnO and TiO_2 have attracted considerable attention due to their non-toxicity, widespread availability, chemical stability, and favorable optical properties [9–11]. These materials are promising candidates for various applications, including optoelectronic devices, sensors, and solar cells, owing to their ability to precisely control material size, shape, and uniformity [12–14]. However, despite their many advantages, the optical performance of pristine ZnO and TiO_2 is limited by a high charge recombination rate [15]. To address this limitation, combining ZnO and TiO_2 to form a heterojunction has emerged as a viable strategy [7,16]. In recent years, heterojunction photocatalysts have gained significant interest from researchers due to their reduced recombination rates [6]. This approach leverages the complementary properties of each material, resulting in broader light absorption (extending into the visible spectrum), reduced electron-hole recombination, improved charge transfer, enhanced stability and durability, and increased photocatalytic activity. Collectively, these improvements significantly enhance the efficiency of heterojunction photocatalysts, particularly in applications such as photocatalytic wastewater treatment [13,17].

Heterojunctions formed from two metal oxides such as ZrO_2, Bi_2O_3, Co_3O_4, Ga_2O_3, Fe_2O_3, Al_2O_3, $BiVO_4$, PbO, CuO, ZnO, Cu_2O, Ta_2O_5, CoO, TiO_2, WO_3, and SnO are characterized by low cost, enhanced stability, and improved visible light utilization. These heterojunctions have been widely applied in energy harvesting, wastewater treatment, air purification, and hydrogen production [18–20]. Among these materials, ZnO and TiO_2 are particularly well-suited for heterojunction formation due to their similar band gaps and closely aligned photocatalytic activities under sunlight irradiation [21–23]. Additionally, doping with noble metals, transition metals, and non-metals has been shown to enhance photocatalytic performance; however, the high cost of noble metals limits their practical use. In contrast, doping with transition metals offers a cost-effective approach to improving photocatalytic efficiency [24,25]. Copper stands out among transition metals due to its high electrical conductivity, ability to reduce the band gap, and overall enhancement of photocatalytic activity [24–26]. Given these advantages and its strong photoactivity, copper was selected as the dopant for synthesizing a ZnO-TiO_2 heterojunction photocatalyst. The sol-gel method is one of the best available synthesis techniques for creating nanomaterials since it doesn't require complicated setups and can be carried out at room pressure as well as temperature. The process of sol-gel synthesis involves hydrolysing and condensing a titanium precursor to create a sol and subsequently a gel. The resulting xerogel is then ground and heated to create extremely crystalline TiO_2 nano powders, following solvent evaporation [27]. Despite numerous reports on TiO_2 and ZnO-based photocatalysts for dye degradation, no study has yet explored the degradation of Turquoise Blue G (TBG) dye using Cu-doped ZnO/TiO_2 heterojunctions. Previous investigations have mainly focused on TiO_2 or ZnO individually or on Cu doped ZnO/TiO_2 systems tested against dyes such as Methylene Blue, Rhodamine B, or Congo Red [28,29].

However, the application of this ternary photocatalyst to TBG - a reactive copper-phthalocyanine dye known for its strong color stability and recalcitrance- has not been reported so far. In this context, the present work introduces a cost-effective sol-gel synthesis of Cu doped ZnO/TiO_2 photocatalysts with varying Cu contents (3-9 wt%) and evaluates their performance for TBG degradation under UV irradiation. The 7 wt% Cu: ZnO/TiO_2 composition demonstrated the highest photocatalytic efficiency, achieving 95% TBG degradation within 150 min, and the Chemical Oxygen Demand (COD) was reduced by 77.78%, decreasing to 22.22% of its initial value compared to the untreated wastewater. This study, therefore, establishes a new application of Cu modified ZnO/TiO_2 heterojunctions for the effective mineralization of TBG dye, addressing a research gap and providing insights into the roles of Cu doping, interfacial charge transfer, and pH conditions on photocatalytic efficiency. Furthermore, the recyclability and stability of the optimized photocatalyst were assessed over multiple reaction cycles, revealing excellent reusability with minimal loss in photocatalytic activity. This comprehensive investigation, therefore, establishes a new application of Cu doped ZnO/TiO_2 heterojunctions for TBG degradation, supported by stability and reusability data that demonstrate the material's potential for practical wastewater treatment applications.

2. Experimental

2.1. Materials

Titanium isopropoxide (TTIP) and cupric nitrate trihydrate (98%) were sourced from Sisco Research Laboratories Pvt. Ltd., Mumbai, India. Zinc acetate dihydrate (98%) was procured from Loba Chemie Pvt. Ltd., Mumbai, India. All chemicals, being of analytical

10.57647/ijc.2026.1601.05

grade, were used without any further purification. Experiments were conducted under ambient conditions, with distilled water used for preparing all aqueous solutions.

2.2. TiO_2 and ZnO solution preparation method

TiO_2 Solution: 0.01 Molar (M) TTIP was added dropwise to 20 ml of ethanol with continuous stirring at 500-600 rpm with the help of a magnetic stirrer at ambient conditions. 3-5 ml pure acetic acid added dropwise into the TTIP solution to maintain pH 3-4 with continuous stirring. A slightly whitish colour solution is observed. Stirr the solution for 5-10 minutes at room temperature. *ZnO Solution:* 0.01 Molar (M) of zinc acetate dihydrate added slowly in 20 ml of ethanol in another beaker, continuously stirring using a magnetic stirrer at 400-500 rpm at room temperature. Added 10 ml water dropwise to completely dissolve zinc acetate dihydrate with stirring, then added 5-10 ml pure acetic acid to maintain pH 3-4 at room temperature. A clear, transparent solution was prepared.

2.3. Synthesis of ZnO/TiO_2 nano-heterojunction photocatalyst by the Sol-Gel method

An added *ZnO solution* in *TiO_2 solution* was dropped at room temperature (RT) with vigorous stirring by a magnetic stirrer. While the addition of *ZnO solution*, the viscosity of *TiO_2 solution* increased. Stir the mixture of both onesolutions for 1 h at ambient conditions. This resulted in a white thick sol and then aged for 24 h. Gel is formed after 24 h of aging. Gel cleaned with distilled water at high rpm in a centrifuge to remove impurities and dried at 100 °C for 2 h. Grinded the dry material and calcined at 500 °C for 2 h. A white fine crystalline photocatalyst was synthesized.

2.4. Synthesis of Cu:ZnO/TiO_2 nano heterojunction photocatalyst by Sol-Gel method

Cu:ZnO Solution: 0.01 M of zinc acetate dihydrate added slowly in 20 ml of ethanol in another beaker, continuously stirring using a magnetic stirrer with 400-500 rpm at room temperature. Added 10 ml water dropwise to completely dissolve zinc acetate dihydrate with stirring, then added cupric nitrate trihydrate (3wt% - 9wt% Cu based on ZnO) slowly while stirring. After completely dissolving cupric nitrate trihydrate, 5-10 ml pure acetic acid was added to maintain a pH of 3-4 at room temperature.

A clear, blue colour, transparent solution was prepared.*Cu:ZnO/TiO_2 Solution:* Added *Cu:ZnO solution* in *TiO_2 solution* dropwise at room temperature with vigorous stirring by magnetic stirrer. Upon the addition of Cu:ZnO solution, the viscosity of the *TiO_2 solution* increased. Stir the mixture of both solutions for 1 h at ambient conditions.

This resulted in a white thick sol and then aged for 24 h. After aging for 24 h, the gel was formed. It was then washed with water at high rpm in a centrifuge to remove impurities and subsequently dried at 100°C for 2 h. Grinded the dry material and calcined at 500 °C for 2 h in a muffle furnace under static air (closed chamber) conditions, without any controlled gas or inert atmosphere.

A slight greenish fine crystalline heterojunction photocatalyst was synthesized. Diagrammatic representation of Cu:ZnO/TiO_2 nano heterojunction photocatalyst synthesis process by sol-gel method shown in Fig. 1.

To analyze and correlate the photocatalytic performance, pure TiO_2, pure ZnO, ZnO/TiO_2, and Cu:ZnO/TiO_2 (3 wt% - 9 wt%) were synthesized separately.

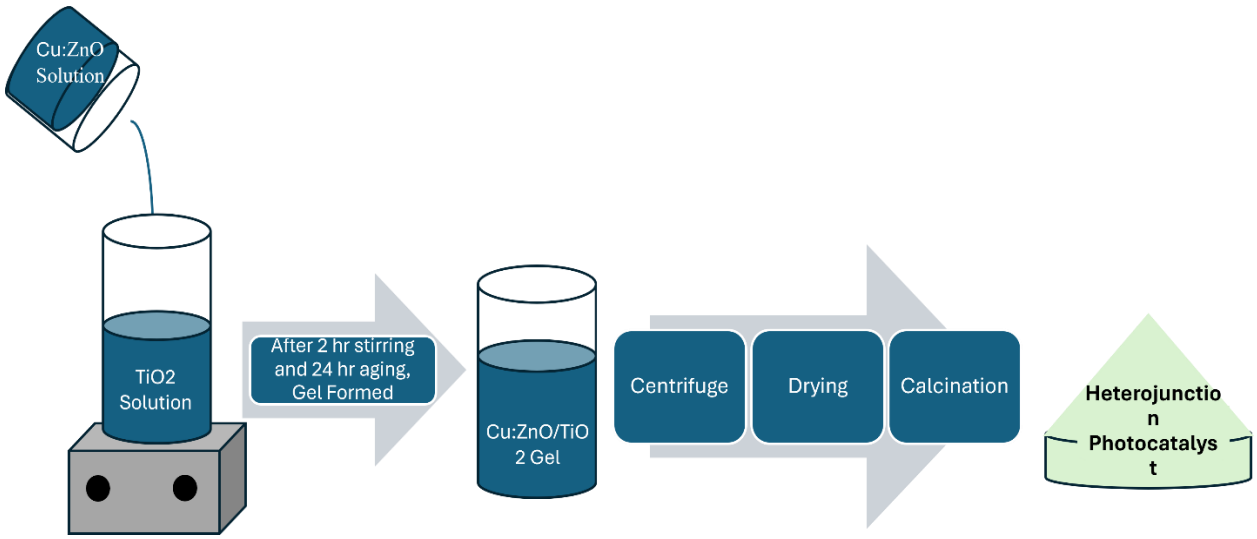

Figure 1. Schematic of Cu:ZnO/TiO_2 nano heterojunction photocatalyst synthesis process by the sol-gel method

10.57647/ijc.2026.1601.05

2.5. Characterization of synthesized nano heterojunction photocatalyst

Optical characterization was conducted with UV-vis spectroscopy (Perkin Elmer, LAMBDA750), and Tauc's relationship was used to calculate the heterojunction photocatalyst's band gap. Structural characteristics and phase shifts of pure TiO_2, pure ZnO, ZnO/TiO_2, and $Cu:ZnO/TiO_2$ photocatalysts were analyzed by X-ray diffraction (XRD) (PANalytical, EMPYREAN, X-Ray Lab, IITB) with Cu Kα radiation (λ = 1.54184 Å). The surface morphology of both pure and doped photocatalysts was analyzed using field emission gun scanning electron microscopy (FE-SEM) (JEOL JSM-7600F, SAIF, IITB). Elemental analysis and mapping of the doped photocatalysts were conducted using energy-dispersive X-ray spectroscopy (EDS) mapping (Apreo 2S Highvac, Thermofisher Scientific).

3. Result and discussion

3.1. Optical Properties- UV-Vis Spectroscopy

UV-Vis spectroscopy was used to characterize pure TiO_2, pure ZnO, ZnO/TiO_2, and $Cu:ZnO/TiO_2$ heterojunction photocatalysts in order to evaluate their optical properties and estimate their band gaps from the absorbance spectra. The absorption spectra were recorded in the wavelength range of 250–650 nm. The pure TiO_2 exhibits an absorption edge around 388.7 nm (corresponding to a band gap of 3.19 eV), while pure ZnO shows an edge near 374.85 nm (~3.308 eV), consistent with reported values for these wide band gap semiconductors. Upon forming the ZnO/TiO_2 heterojunction, a slight red shift in the absorption edge to 384 nm (3.23 eV) is observed, indicating improved interfacial charge transfer and band alignment between ZnO and TiO_2. With Cu incorporation, the absorption edge shifts further toward the visible region. This red shift becomes more pronounced with increasing Cu content, signifying enhanced visible-light absorption and band gap narrowing in the Cu doped composites. To quantify this change, the reflectance spectra (R) were converted into the Kubelka–Munk function, expressed as:

$$F(R_\infty) = \frac{(1-R_\infty)^2}{2R_\infty} \quad (1)$$

where R_∞ is the reflectance of an optically thick sample. Under the Kubelka–Munk theory, F(R) is proportional to the absorption coefficient (α) assuming constant scattering across wavelengths. This relationship allows the optical band gap to be evaluated using the Tauc relation:

$$[F(R)\,h\nu]^{1/n} = k(h\nu - Eg) \quad (2)$$

Where k is a constant, $h\nu$ is the photon energy, and n = 1/2 for direct transitions, respectively. The corresponding Tauc plots for all samples are shown in Fig. 2. The calculated band gap values were found to be 3.19 eV (TiO_2), 3.308 eV (ZnO), 3.23 eV (ZnO/TiO_2), and 3.0 eV (optimized 7% $Cu:ZnO/TiO_2$). The progressive decrease in Eg from TiO_2 → ZnO → ZnO/TiO_2 → 7% $Cu:ZnO/TiO_2$ demonstrates that heterojunction formation and Cu doping both contribute to band gap narrowing and visible-light activation

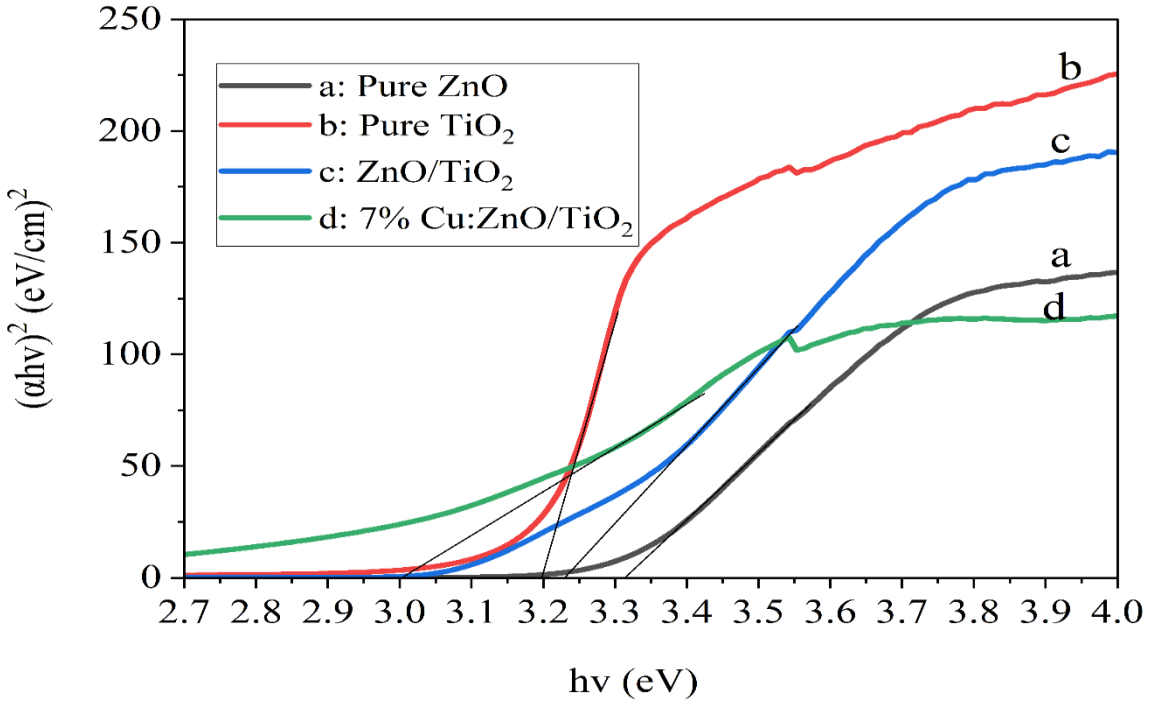

Figure 2. Tauc's plot for pure TiO_2, pure ZnO, ZnO/TiO_2, and optimized 7wt% $Cu:ZnO/TiO_2$ heterojunction photocatalyst

10.57647/ijc.2026.1601.05

The Cu dopant introduces localized energy levels near the conduction band edge, facilitating sub-band transitions and extending light absorption into the visible region [30,31]. In summary, the DRS analysis clearly shows a sequential band gap reduction from pure TiO_2 and ZnO to the optimized 7% Cu:ZnO/TiO_2 heterostructure. The synergistic effects of heterojunction formation and Cu doping enhance visible-light absorption and charge separation efficiency, in agreement with the XPS and photocatalytic performance results. This finding is significant, as it demonstrates that a reduced band gap can substantially increase visible light absorption, potentially leading to more efficient photocatalytic degradation of wastewater using heterojunction materials.

3.2. Structural properties- X-Ray diffraction (XRD)

The structural characteristics of the synthesized heterojunction photocatalysts were further investigated using X-ray diffraction (XRD). Fig. 3 shows the XRD patterns of both the heterojunction and the pure photocatalysts. The XRD data were recorded over a 2θ range of 10–80°. The patterns confirm the presence of a crystalline anatase structure for TiO_2 and a hexagonal wurtzite structure for ZnO [17]. For pure TiO_2, characteristic diffraction peaks were observed at 2θ values of 25.3°, 36.9°, 37.8°, 48°, 53.9°, 55°, 62.7°, 68.66°, 70.8°, and 74.9° corresponding to the (101), (103), (004), (200), (105), (211), (204), (116), (220) and (215) lattice planes, respectively, in accordance with JCPDS file No. 73-1764 [19,32]. Similarly, for ZnO, peaks located at 31.97°, 35.10°, 36.4°, 47.81°, 56.8°, and 62.60° correspond to the (100), (002), (101), (110), and (103) planes, respectively, as per JCPDS file No. 036-1451 [32,33]. In addition, peaks attributed to copper (Cu_2O and CuO) were observed at 29.77°, 36.89°, 42.32°, and 61.3°, corresponding to the (110), (111), (200), and (220) planes, respectively, according to JCPDS file No. 00-05-0667 and No. 00-48-1548 [34,35]. These results confirm the successful formation of ZnO/TiO_2 heterojunction composites as well as the incorporation of copper onto the ZnO/TiO_2 heterojunction. Furthermore, the crystallite sizes of all synthesized photocatalysts were estimated using the Debye-Scherrer equation (Equation 3), which is commonly employed to calculate the crystal size of nanoparticles [24].

$$D = K\lambda/(\beta * Cos\theta) \quad (3)$$

Here, θ is the Bragg diffraction angle (in radians), D represents the average crystallite size, K is the Scherrer constant (typically 0.9), β is the full width at half maximum (FWHM) of the diffraction peak (in radians), and λ is the wavelength of the incident X-ray. The calculated crystallite sizes of the prepared photocatalysts were 24.97 nm for pure TiO_2, 29.49 nm for ZnO/TiO_2, and 36.08 nm for 7% Cu:ZnO/TiO_2. These values confirm the successful synthesis of nanostructured photocatalysts, both pure and heterojunction types. The observed increase in crystallite size suggests the successful formation of the ZnO/TiO_2 heterojunction and the effective incorporation of copper into the ZnO/TiO_2 crystal structure [17,36,37].

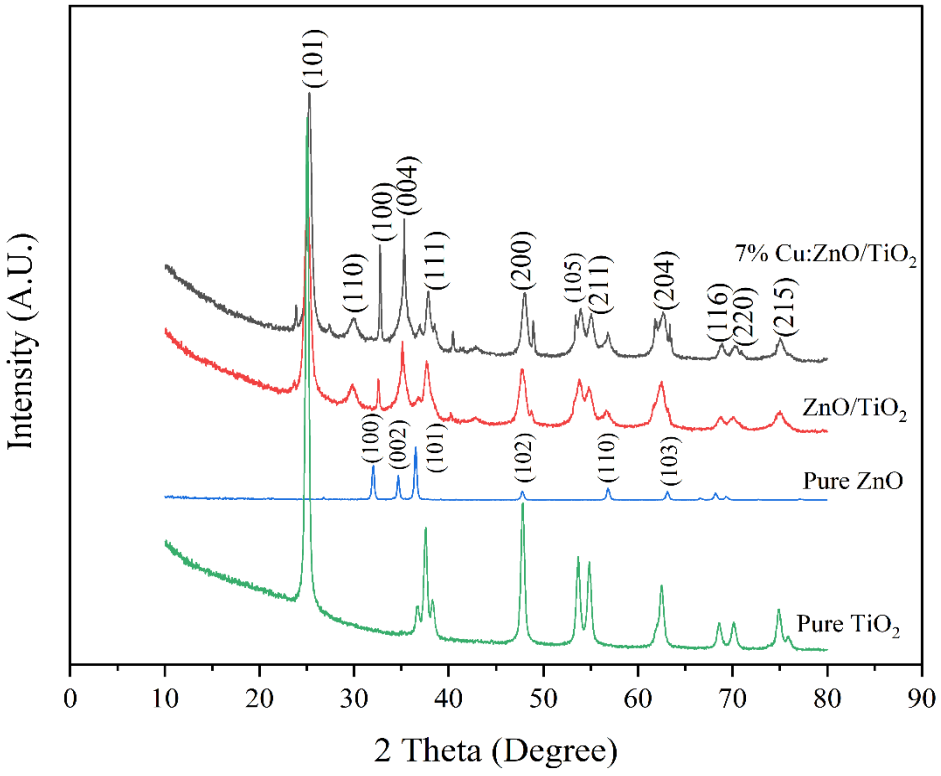

Figure 3. XRD plot of synthesized pure TiO_2, pure ZnO, ZnO/TiO_2, and 7% Cu:ZnO/TiO_2

10.57647/ijc.2026.1601.05

3.3. Morphological properties- field emission scanning electron microscopy (FE-SEM) and EDS analysis

Fig. 4(a–d) shows the surface morphology of the prepared pure TiO_2, pure ZnO, ZnO/TiO_2, and 7% $Cu:ZnO/TiO_2$ heterojunction photocatalysts, examined using field emission scanning electron microscopy (FE-SEM). The analysis confirmed that all synthesized catalysts exhibit an almost spherical shape with a uniform size distribution [38]. In Fig. 4(d), the presence of copper on the ZnO/TiO_2 surface is suggested, although it is not clearly visible in the SEM image due to the low concentration of the dopant. Previous studies have reported that copper doping can enhance the surface morphology, crystallite size, and atomic arrangement of photocatalysts [9,22,38,39].

As a result, the highest photocatalytic degradation efficiency was observed for the 7% $Cu:ZnO/TiO_2$ photocatalyst among all the prepared samples. Energy-dispersive X-ray spectroscopy (EDS) mapping analysis was used to evaluate the elemental distribution. For the 7% $Cu:ZnO/TiO_2$ sample, the results are shown in Fig. 5 and 6(e–h). EDS elemental analysis of the 7% $Cu:ZnO/TiO_2$ photocatalyst (Fig.5) confirmed the uniform presence of Ti, O, Zn, and Cu. The Cu content measured at 6.6 wt% closely matches the intended 7 wt% doping. The corresponding atomic percentages were 74.1% O, 22.2% Ti, 0.8% Zn, and 3.0% Cu, confirming successful incorporation of Cu into the ZnO/TiO_2 heterostructure.

Furthermore, the presence of Cu, O, Ti and Zn in the photocatalyst was confirmed by the element distribution, which is represented by colored dots in the mapping images Fig. 6(e–h). The 7% $Cu:ZnO/TiO_2$ catalyst looks to be homogenous based on the EDS mapping [39].

3.4. Fourier transform infrared spectroscopy (FTIR) analysis

FTIR spectroscopy is a valuable technique for analyzing the chemical composition of compounds. The FTIR spectra of sol-gel synthesized pure TiO_2, pure ZnO, ZnO/TiO_2, and 7% $Cu:ZnO/TiO_2$ are shown in Fig. 7, covering the wavenumber range from 400 cm^{-1} to 4000 cm^{-1}. Several prominent absorption peaks are observed in the spectra of the catalysts.

A broad absorption band in the range of 3200-3600 cm^{-1} (centered at 3454.51 cm^{-1}) corresponds to O-H stretching vibrations, indicating the presence of surface hydroxyl groups and adsorbed moisture. The band at 1632 cm^{-1} is attributed to O-H bending.

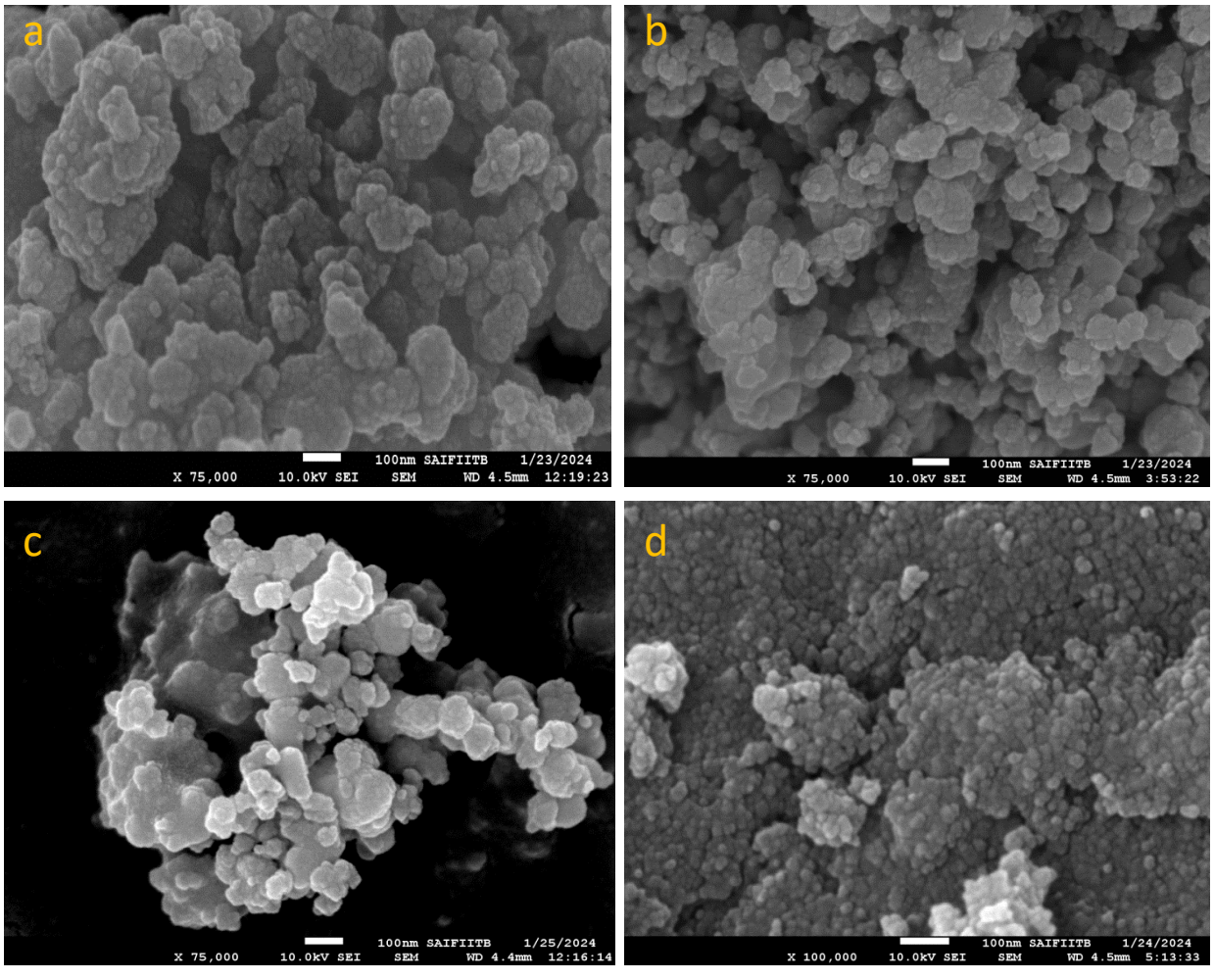

Figure 4. FE-SEM of synthesized a) Pure TiO_2 b) Pure ZnO c) ZnO/TiO_2 d) 7% $Cu:ZnO/TiO_2$

10.57647/ijc.2026.1601.05

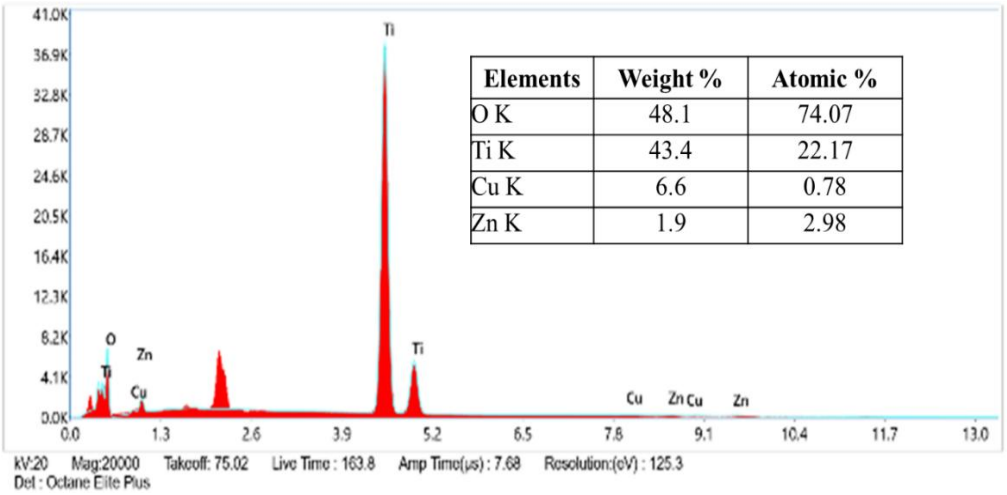

Elements	Weight %	Atomic %
O K	48.1	74.07
Ti K	43.4	22.17
Cu K	6.6	0.78
Zn K	1.9	2.98

Figure 5. EDS of synthesized 7% Cu:ZnO/TiO_2 nano heterojunction photocatalyst

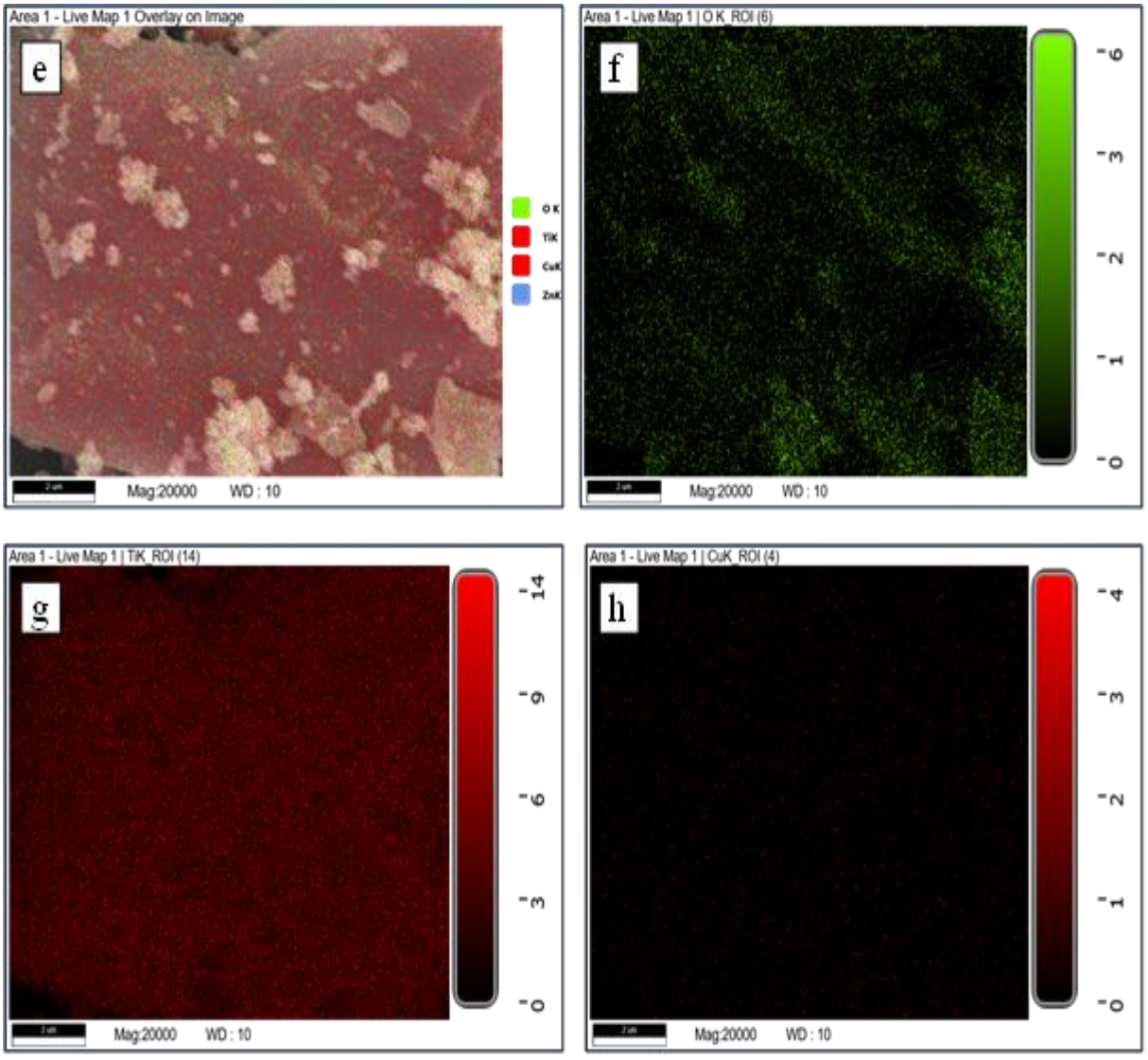

Figure 6. EDS Elemental mapping (e-h) of 7% Cu:ZnO/TiO_2

The peak at 1400 cm^{-1} is associated with Ti-O-Ti stretching. A strong peak at 661 cm^{-1} is characteristic of Ti-O stretching vibrations in TiO_2 [40], while the band at 538 cm^{-1} corresponds to Zn-O metal-oxygen vibrations. The absorption peak at 1079 cm^{-1} is corresponds to C-N or C-O stretching vibrations [41]. In the ZnO/TiO_2 composite, the O-H stretching mode originating from $Zn(OH)_2$ or free O-H groups suggests bond disruption caused by ZnO particles.

10.57647/ijc.2026.1601.05

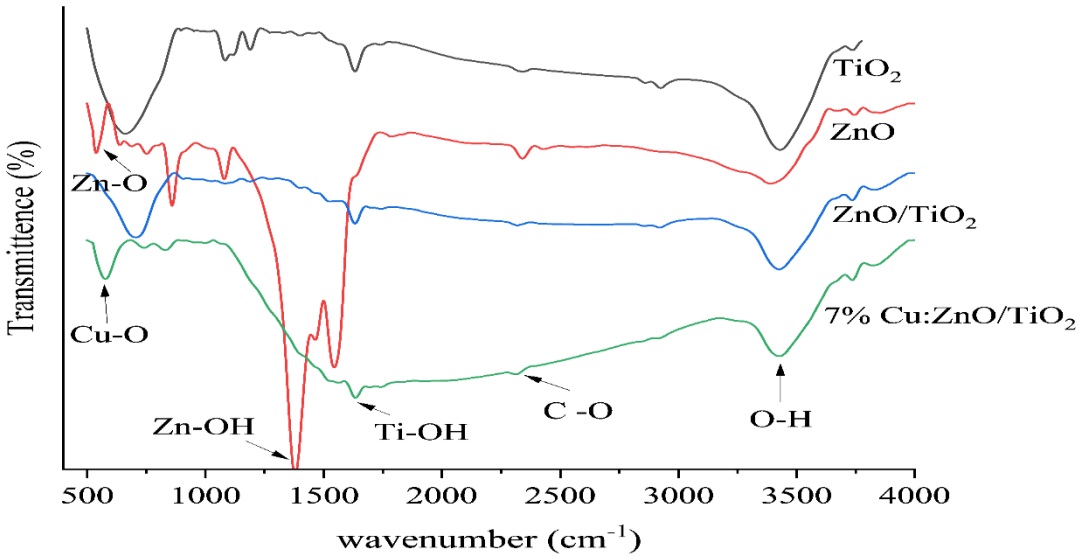

Figure 7. FTIR of synthesized pure TiO_2, pure ZnO, ZnO/TiO_2 and 7%Cu:ZnO/TiO_2

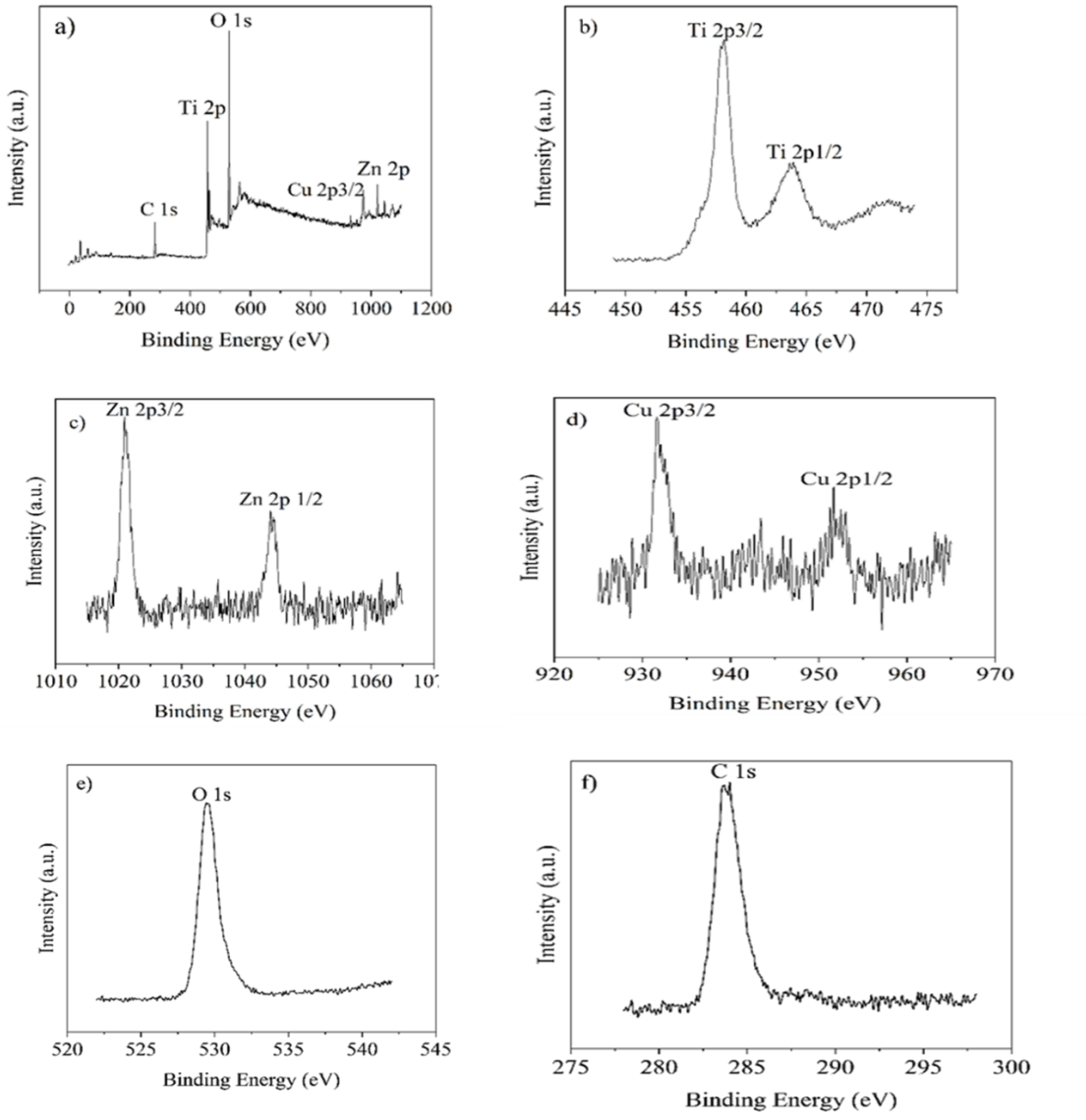

Figure 8. XPS analysis of 7% Cu:ZnO/TiO_2 heterojunction photocatalyst a) Survey b) Ti 2p peak c) Zn 2p peak d) Cu 2p e) O1s peak f) C1s peak

10.57647/ijc.2026.1601.05

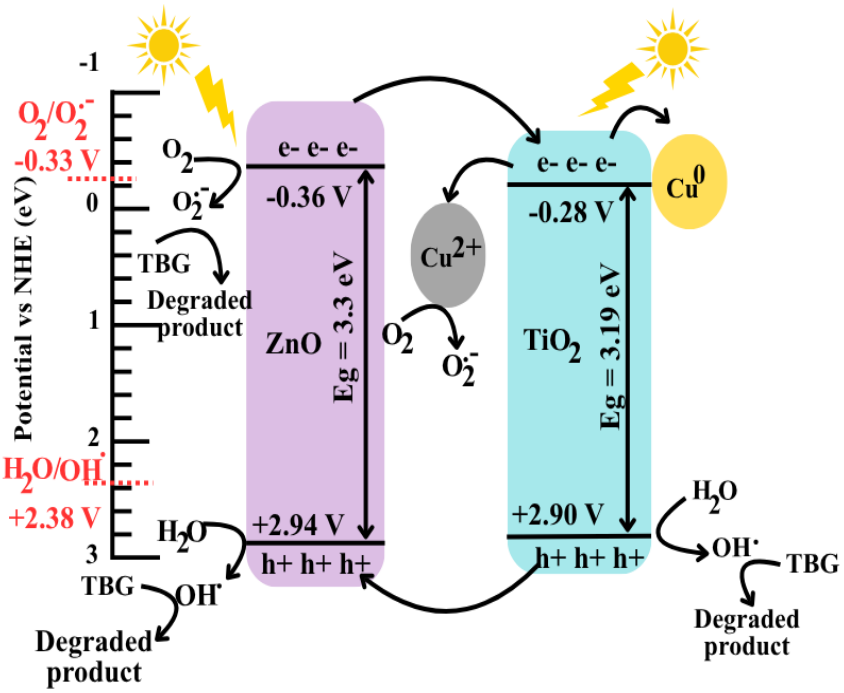

Figure 9. Schematic energy band alignment of the 7% Cu:ZnO/TiO_2 heterojunction photocatalyst with band edge

Symmetric and asymmetric stretching vibrations of zinc carboxylate appear at 1632 cm^{-1}, while a band at 3426 cm^{-1} indicates the presence of tetrahedral vacancies in Ti^{4+}-OH groups [20], confirming the formation of the ZnO/TiO_2 composite.

For the 7% Cu:ZnO/TiO_2 photocatalyst, FTIR analysis reveals stretching modes corresponding to Ti-O, C-H, C-O, ZnO, and Ti-OH, along with a distinct Cu-O vibration near 600 cm^{-1}, confirming the presence of copper [37]. The observed shift in vibrational frequencies suggests the substitution of Cu^{2+} into the Zn-O lattice, consistent with established vibrational mode theories in mixed crystals [42].

These findings confirm the successful synthesis of a Cu:ZnO/TiO_2 heterojunction photocatalyst via the sol–gel method.

3.5. X-ray photoelectron spectroscopy (XPS) analysis

XPS analysis of the material's elemental composition and chemical states is shown in Fig. 8.

The XPS survey spectrum in Fig. 8(a) confirms the presence of Ti, Zn, O, Cu, and C in the photocatalyst. The Ti 2p spectrum in Fig. 8(b) exhibits two characteristic binding energy peaks at 458.16 eV and 464.07 eV, corresponding to Ti $2p_{3/2}$ and Ti $2p_{1/2}$, respectively, indicating the presence of Ti^{4+} in TiO_2 while the Zn 2p spectrum in Fig. 8(c) shows two peaks at 1020.92 eV and 1044.08 eV, attributed to Zn $2p_{3/2}$ and Zn $2p_{1/2}$, respectively, conform the presence of Zn^{2+} in ZnO [32,43,44]. The Cu 2p spectrum shows peaks in Fig. 8(d). at 931.6 eV and 951.68 eV corresponding to Cu $2p_{3/2}$ and Cu $2p_{1/2}$ along with weak satellite features, indicating the existence of Cu^{2+} species on the surface of the composite. The O 1s high-resolution spectrum shown in Fig. 8(e) exhibits a prominent peak centered at 529.43 eV, attributed to lattice oxygen (O^{2-}) associated with Ti-O and Zn-O bonds in the TiO_2 and ZnO lattices, respectively. The C 1s spectrum in Fig. 8(f) shows a peak at 284.02 eV, which corresponds to adventitious carbon used for calibration of the binding energy scale [36]. These XPS results collectively confirm the successful incorporation of Cu into the ZnO/TiO_2 heterojunction structure without altering the oxidation states of Zn and Ti. The coexistence of Zn^{2+}, Ti^{4+}, Cu^{2+}, and O^{2-} species suggests intimate interfacial contact between the components, facilitating efficient charge transfer within the heterostructure.

3.6. Reaction mechanism of TBG dye degradation by 7% Cu:ZnO/TiO_2 heterojunction photocatalyst

The degradation of TBG dye over the 7% Cu:ZnO/TiO_2 heterojunction mainly proceeds through the generation of superoxide radicals ($O_2^{\cdot-}$), while hydroxyl radicals ($^{\cdot}OH$) and valence-band holes (h^+_{VB}) also contribute to the oxidation pathway. Upon light exposure, both ZnO and TiO_2 absorb photons and produce electron-hole pairs [45]. Because the conduction band of ZnO lies at a slightly higher energy (more negative potential) than that of TiO_2, the excited electrons can easily migrate from ZnO to TiO_2, whereas the photogenerated holes move in the opposite direction. This stepwise transfer of charge carriers represents a Type-II heterojunction, which effectively

decreases electron–hole recombination and accelerates redox reactions on the catalyst surface [46–48].

3.6.1. *Role of copper species in redox and possible plasmonic contribution*

Copper acts in two complementary ways to enhance photocatalytic performance:

Redox-mediated charge trapping: Cu^{2+} ions that are either embedded within the ZnO lattice or anchored at the ZnO/TiO_2 interface behave as temporary electron acceptors. During irradiation, these ions are reduced to Cu^{+}, storing photogenerated electrons and preventing their direct recombination with holes. The trapped electrons can subsequently reduce dissolved oxygen, producing reactive $O_2^{\bullet-}$ radicals while regenerating Cu^{2+}. This reversible Cu^{2+} /Cu^{+} cycle promotes continuous charge transfer and radical generation throughout the reaction [49–52].

Plasmonic and interfacial effects of metallic Cu^0: A minor quantity of metallic copper particles may develop during synthesis. These Cu^0 nanoparticles exhibit localized surface plasmon resonance (LSPR) under UV or near-visible illumination. The LSPR process broadens the spectral response of the composite and produces energetic electrons that can be injected into the conduction band of TiO_2 or ZnO. In addition, metallic Cu functions as an electron sink through a Schottky-type interface, further facilitating electron migration toward adsorbed oxygen molecules to yield $O_2^{\bullet-}$ radicals [53,54]. The cooperative influence of these redox and plasmonic pathways, together with the Type-II band alignment between ZnO and TiO_2, accounts for the superior photocatalytic activity observed for the 7% Cu:ZnO/TiO_2 sample. The overall mechanism, including charge transfer and radical generation, is summarized in Fig. 9. The proposed interpretation is consistent with earlier investigations of Cu-modified ZnO/TiO_2 systems reported in the literature [55,56].The following reactions demonstrate the reactions taking place at the conduction band of the photocatalyst:

$$\text{Photocatalyst (Cu:ZnO/TiO}_2\text{)} + h\nu \longrightarrow \text{Photocatalyst } (e^-_{CB} + h^+_{VB}) \quad (4)$$

$$e^-_{CB} + O_2 \longrightarrow O_2^{\cdot-} \quad (5)$$

$$h^+_{VB} + H_2O \longrightarrow OH^{\cdot} \quad (6)$$

$$\text{TBG} + h^+_{VB} / OH^{\cdot} / O_2^{\cdot-} \longrightarrow \text{Degraded Product} \quad (7)$$

positions referenced to the normal hydrogen electrode (NHE). The diagram illustrates the conduction band (E_{CB}) and valence band (E_{VB}) potentials of ZnO and TiO_2, showing electron transfer from the ZnO conduction band to TiO_2 and hole migration in the opposite direction under light irradiation, leading to efficient charge separation and enhanced photocatalytic activity.

3.7. Photocatalytic degradation study of turquoise blue G (TBG) dye

Fig. 10 shows the experimental setup used for turquoise blue G dye degradation exposed to UV rays. Fig. 11 gives the photocatalytic degradation profiles of 1 liter of 20 ppm turquoise blue G dye using 0.5 gm weight of all synthesized pure and heterojunction photocatalyst under medium pressure mercury vapor (MPMVL) 150-watt UV light source. All of the synthesized photocatalyst's degrading performance was evaluated against the commercial Degussa P-25. In the presence of UV light, pure TiO_2 degraded in minor amounts of turquoise blue G solution.

In contrast, ZnO/TiO_2 and Cu:ZnO/TiO_2 photocatalyst calcined at 500°C demonstrated improved photodegradation than pure TiO_2, while 7% Cu:ZnO/TiO_2 showed significant enhancement, achieving a C/C_0 value of approximately 0.05 after 2.5 hours, which is 1.52 times higher than pure TiO_2.

This indicates that 7% Cu:ZnO/TiO_2 effectively enhances the photoactivity compared to pure TiO_2 alone. Specifically, the 7% Cu:ZnO/TiO_2 formulation consistently displayed lower C/C_0 values across various reaction durations, indicating superior degradation performance.

Notably, 7% Cu:ZnO/TiO_2 demonstrated the highest degradation efficiency among all synthesized photocatalysts. Within the initial 0.5 hours, 7% Cu:ZnO/TiO_2 degraded 70% of the dye, whereas commercial Degussa P-25 achieved only 65% degradation.

Therefore, among all the synthesized photocatalysts tested in the presence of UV light, 7% Cu:ZnO/TiO_2 attained the highest degradation efficiency of 95%. Fig. 12 illustrates the nearly clean water that was obtained after 150 minutes of photocatalytic treatment with 7% Cu:ZnO/TiO_2. The following formula is used to determine the photodegradation efficiency.

$$Photodegradation\ efficiency\ (\%) = \frac{Intial\ Concentration - Final\ Concentration}{Intial\ Concentration} x100 \quad (8)$$

10.57647/ijc.2026.1601.05

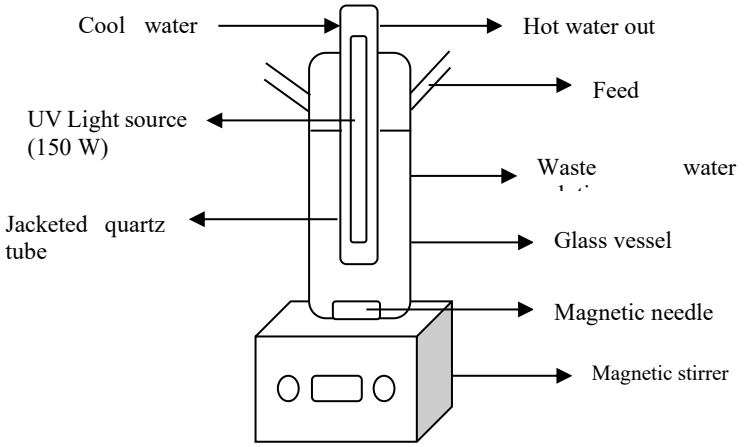

Figure 10. Schematic of the photocatalytic reactor utilized for the degradation of turquoise blue G dye

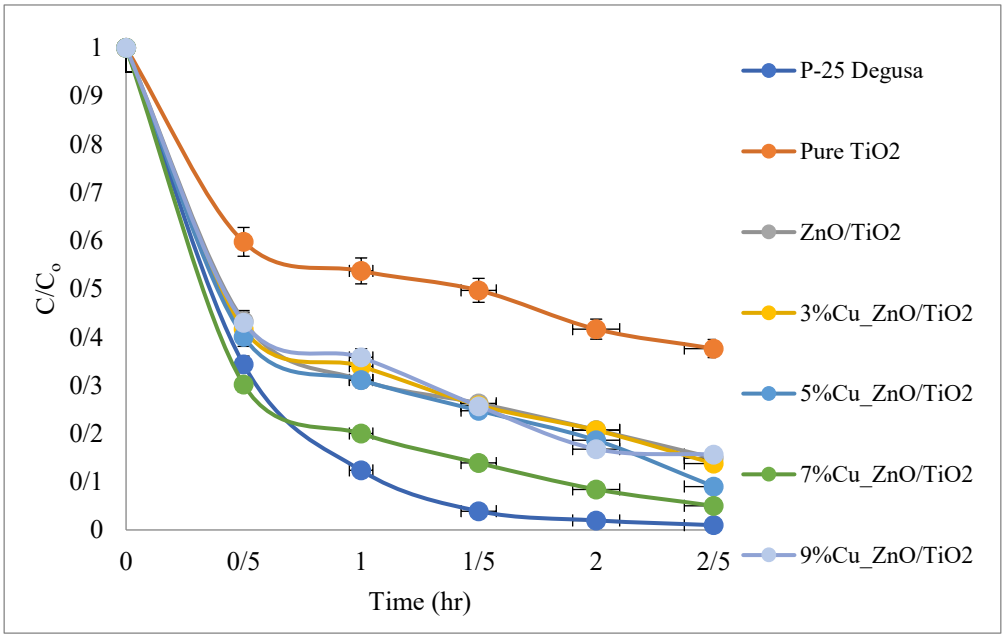

Figure 11. Photocatalytic degradation of turquoise blue G dye using different Cu:ZnO/TiO_2 varied copper dopant (3%, 5%, 7% & 9%), pure TiO_2, ZnO/TiO_2 composite, and Degussa P-25

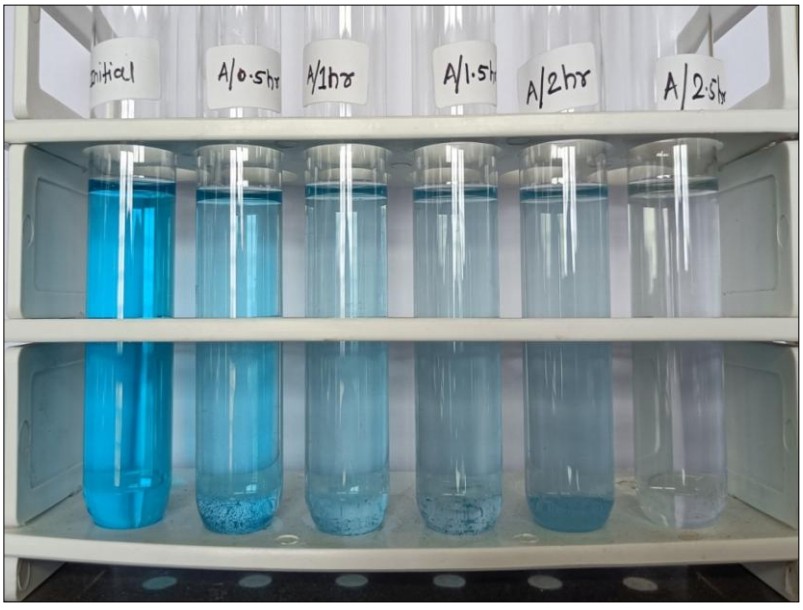

Figure 12. Photocatalytic degradation condition of turquoise blue G dye was assessed using 7% Cu:ZnO/TiO_2 after every 0.5 hour

10.57647/ijc.2026.1601.05

3.8. Chemical oxygen demand (COD) measurement

One common technique for determining the amount of organic matter in waste water is the COD treatment method. The COD of the turquoish blue dye waste water was estimated initially and after the photocatalytic treatment. COD of dye wastewater treated by synthesized pure TiO2, pure ZnO, heterojunction ZnO/TiO2, and Cu:ZnO/TiO2 (3wt% - 9wt%), and compared with the COD value treated by commercial Degussa P-25. The decrease in COD values of the dye solution after treatment suggests that the dye molecules have undergone degradation.

Table 1. Comparative table of photodegradation of turquoise blue (TBG / RTB / TBD) by different photocatalysts

Sr. No.	Photocatalyst	Synthesis Method	Dye	Light source and power (W)	Degradation efficiency (%)	Time	Key notes	References
1	TiO_2 / rGO / g-C_3N_4 nanocomposite immobilized in polystyrene floating films	Solvent casting	Remazol Turquoise Blue (RTB)	Solar Light	60%	1.5 h	Immobilized floating film; recyclability and air-lift reactor configuration studied.	[57]
2	TiO_2 entrapped PVDF photocatalytic membrane	TiO_2 entrapped in PVDF membrane (NIPS method)	Remazol Turquoise Blue (RTB)	UV (TUV 15 W/G15 T8)	variable (depending on operating conditions)	Varies (depending on operating conditions)	Analyzed effects of catalyst loading, pH, dye conc., and addition of H_2O_2 - useful for process comparisons.	[58]
3	ZnO, Al/ZnO, and W/Ag/ZnO nanocomposites	Chemical synthesis of ZnO-based composites	Turquoise Blue Dye (TBD)	UV / simulated sunlight	variable (depending on operating conditions)	2 h	Demonstrates ZnO family materials are active for Turquoise Blue variants; doping/composites improve performance.	[59]
4	AgNP-assisted photocatalyst	Kecemcem leaf extract	Turquoise Blue dye	UV lamp (50 W)	94.57%	2.5 h	Shows AgNP addition enables >94% removal at higher dye concentration (125 mg/L) in lab tests.	[60]
6	TiO_2 immobilized in xanthan gum (TiO_2/XG)	Sol–gel dip-coating technique	Reactive red (RR) and Reactive turquoise (RT) dyes	Solar Light	Reactive Red (RR) dye-92.5% and Reactive turquoise (RT) -90.8%	2 h	Shows solar-driven performance with xanthan biopolymer binder; demonstration of practical solar treatment.	[61]
7	7% Cu:ZnO/TiO_2 heterojunction (Type II)	Room temperature sol-gel (RTSG) method	Turquoise Blue G (TBG)	MPMVL UV lamp (150 W)	95% (fresh photocatalyst) and 84.3% (Recycled photocatalyst)	2.5 h	Novel photocatalyst first time degrades TBG with high efficiency 95% and COD is reduced =77.78% corresponding to 22.22% from its initial value; Reaction Kinetics, pH study, optimized Cu doping, recyclability of photocatalyst (efficiency-84.3%) tested.	This Work

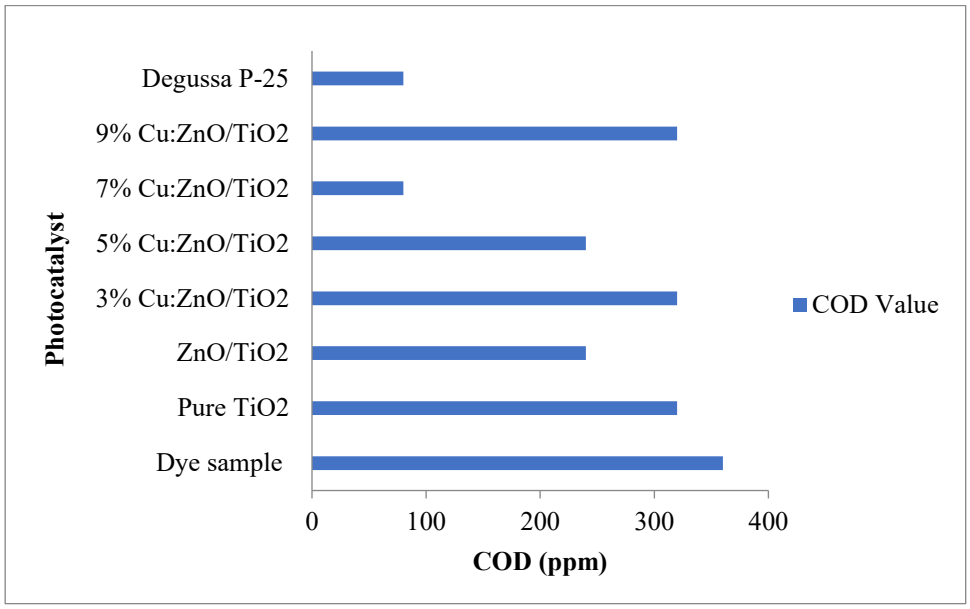

Figure 13. COD of turquoise blue wastewater treated by a synthesized photocatalyst and commercial Degussa P-25

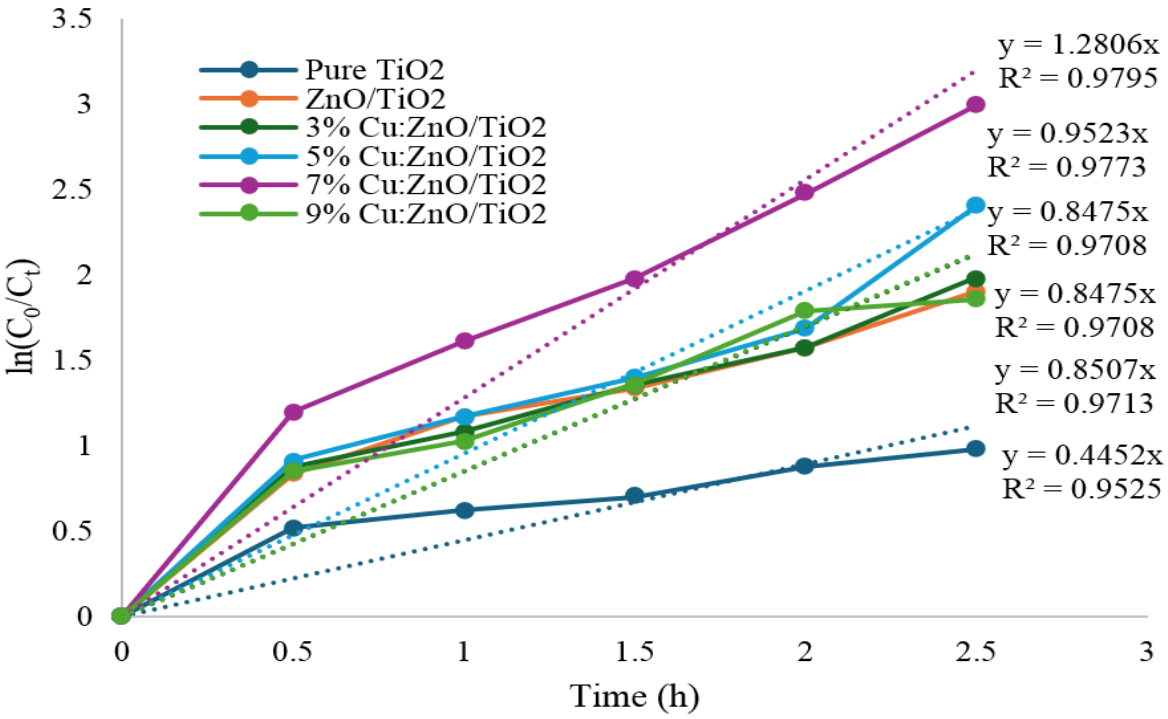

Figure 14. Reaction kinetic study for the degradation of TBG dye by the synthesized photocatalyst

Fig. 13 shows that among all synthesized photocatalysts, the 7% Cu:ZnO/TiO_2 sample exhibited the highest COD removal efficiency of 77.78%, reducing the COD of TBG wastewater from 360 ppm to 80 ppm, corresponding to 22.22% of its initial value. 7% Cu:ZnO/TiO_2 heterojunction photocatalyst degrades as the same as commercial Degussa P-25 and shows the same COD result in Fig. 13.

The COD degradation efficiency is calculated from the following equation.

$$COD\ Reduction\ (\%) = \frac{Intial\ COD - Final\ COD}{Intial\ COD} x100 \quad (9)$$

Table 1 compares representative reported performances for the photocatalytic degradation of Turquoise Blue (TBG) dyes using different catalyst systems reported in the literature and the present study. The literature demonstrates that TiO_2 and ZnO-based materials (including doped and composite forms) can achieve high color removal for Turquoise Blue variants, but reported reaction times and conditions vary widely depending on catalyst form (immobilized membrane, powder, supported nanoparticles), doping/composite strategy, dye concentration, light source, and photon flux.Importantly, no prior published study was found that applies Cu doped ZnO/TiO_2 heterojunctions specifically

10.57647/ijc.2026.1601.05

to Turquoise Blue G (TBG) under the same systematic optimization and recyclability testing reported here making the present 7 wt% Cu:ZnO/TiO_2 study (95% degradation in 150 min, with strong 77.78% COD reduction (corresponding to 22.22% from its initial value and demonstrated recyclability) a novel contribution.

3.9. Reaction Kinetics

Degradation of TBG dye by photocatalysis was described by a pseudo-first-order kinetic model.

$$-\frac{dC}{dt} = kC \quad (10)$$

After integrating equation --well-known pseudo first order (PFO) kinetic model, presented as equation

$$Ct = C0 * e^{(-k1t)} \quad (11)$$

Equ. (10) can be rewritten in a linear form (12)

$$\ln Co/Ct = k1 * t \quad (12)$$

Where, TBG dye concentrations at time t and 0 (initial) are denoted by C_t and C_o, respectively. Reaction time is represented by t in hours, whereas the reaction rate constant is represented by k (h^{-1}) [62].

All prepared photocatalysts showed approximately linear plots between ln (C_o/C_t) and time (h), for the degradation of TBG dye, indicating pseudo-first-order reaction kinetics. The values of rate constant (k) and R^2 are mentioned in Fig. 14 and Table 2.

Table 2. Kinetics data of all synthesized photocatalyst

Sr. No	Synthesized Photocatalyst	Time (h)	k (h^{-1})	R^2
1	Pure TiO_2	2.5	0.4452	0.9525
2	ZnO/TiO_2	2.5	0.8475	0.9708
3	3% Cu:ZnO/TiO_2	2.5	0.8475	0.9708
4	5% Cu:ZnO/TiO_2	2.5	0.9523	0.9773
5	7% Cu:ZnO/TiO_2	2.5	1.2806	0.9795
6	9% Cu:ZnO/TiO_2	2.5	0.8507	0.9713

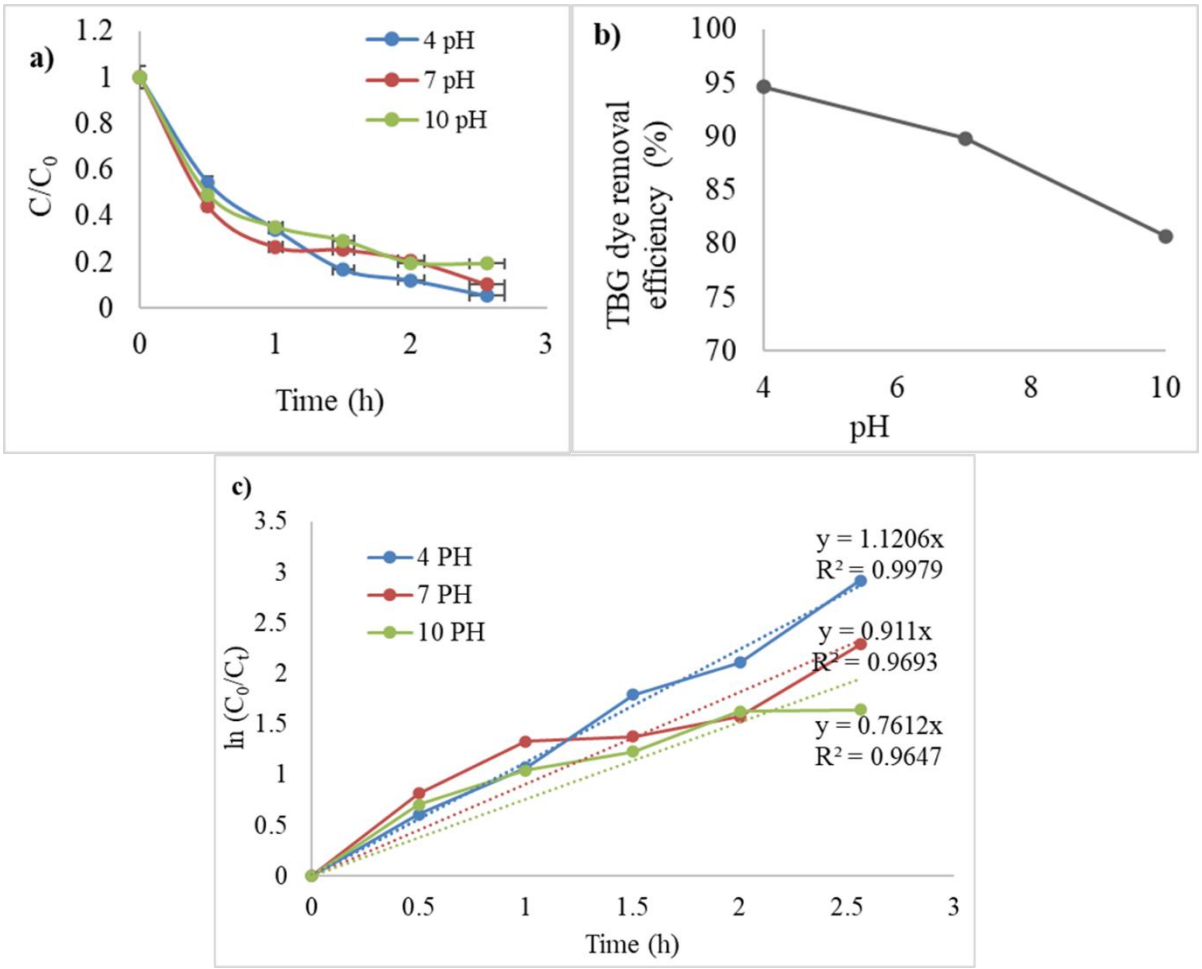

Figure 15. Photodegradation of TBG dye by 7% Cu:ZnO/TiO_2 photocatalyst a) disappearance of TBG dye by photocatalysis at pH 4, 7 and 10 b) TBG dye removal efficiency (%) indicating that acidic conditions favour degradation due to enhanced electrostatic attraction between the positively charged catalyst surface (pH < pHpzc) and anionic dye molecules at pH 4, 7 and 10 c) kinetic analysis of TBG dye at different pH value (4, 7 and 10)

10.57647/ijc.2026.1601.05

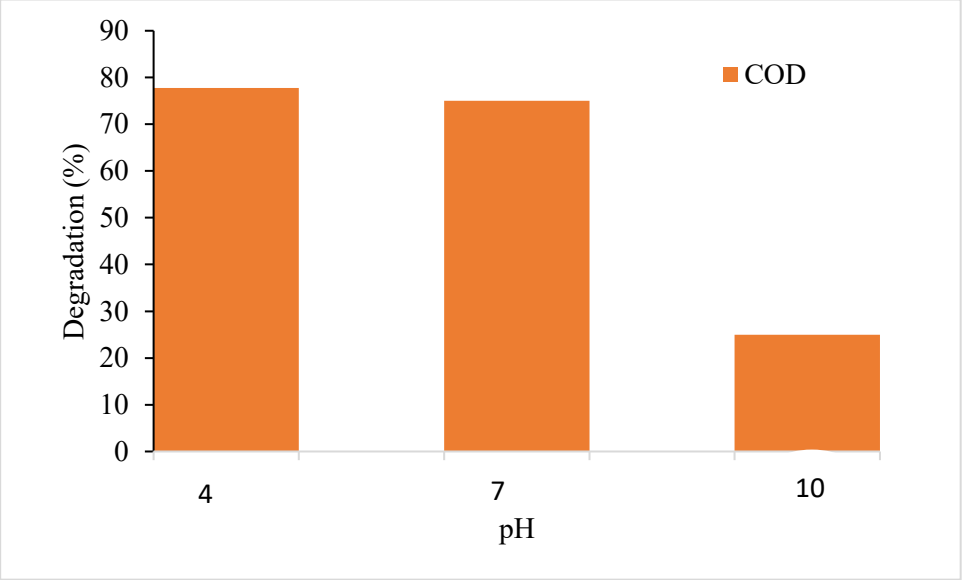

Figure 16. COD study of photodegradation of TBG dye by 7% Cu: ZnO/TiO_2 at 4, 7 and 10 pH

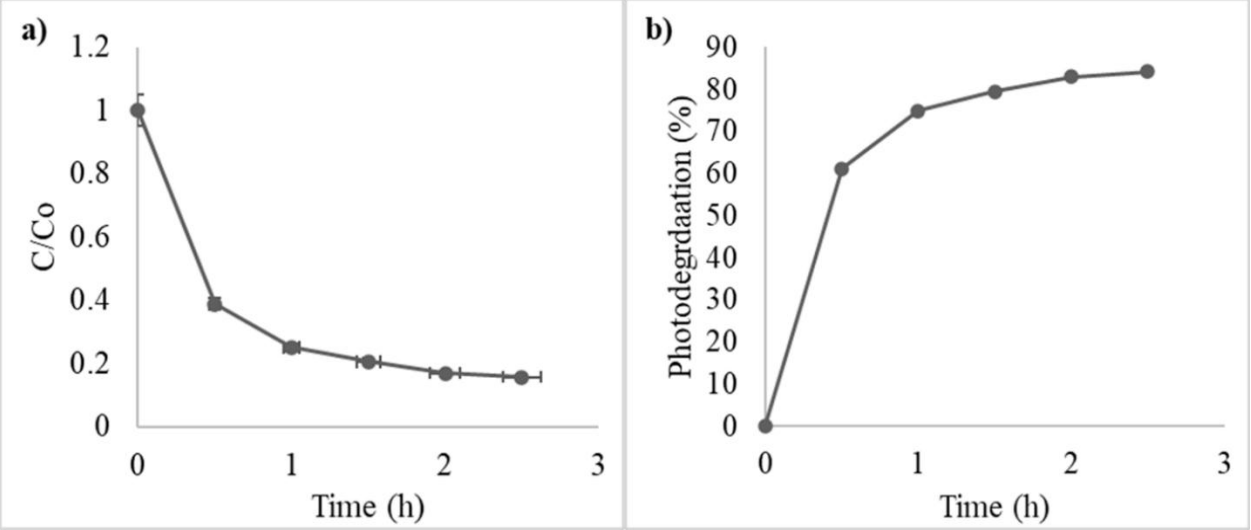

Figure 17. Photocatalytic degradation and recyclability performance of 7% Cu: ZnO/TiO_2 nanophotocatalyst during TBG dye degradation under UV–visible irradiation: (a) variation of normalized concentration (C/C_0) with irradiation time and (b) corresponding photodegradation efficiency (%)

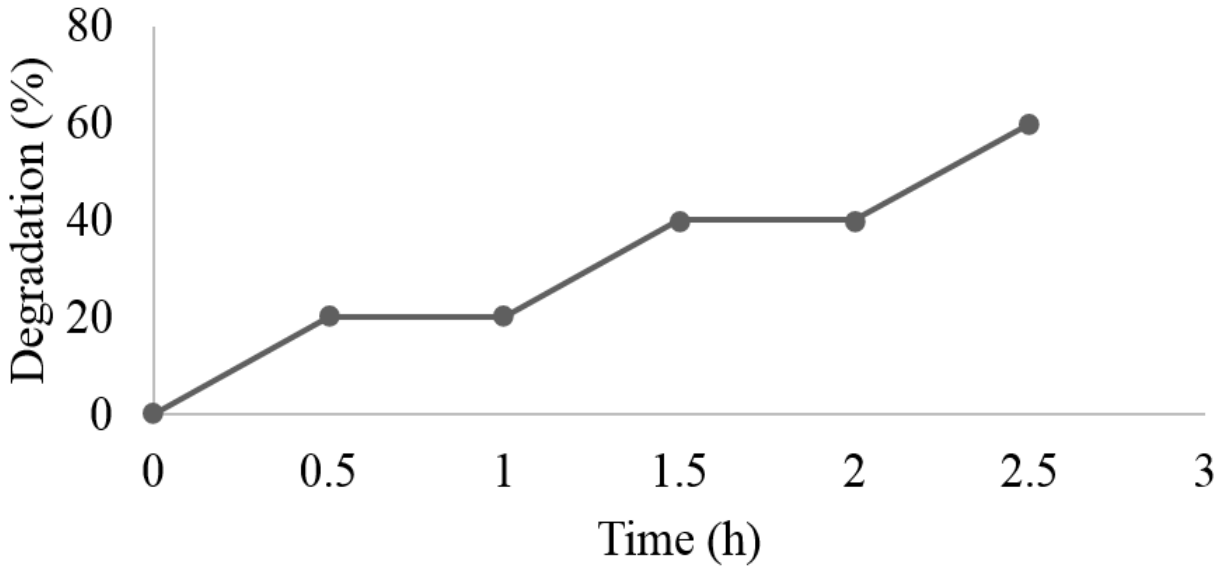

Figure 18. COD study of TBG dye degradation by recycled 7% Cu: ZnO

3.10. Effect of pH on TBG dye degradation

The effectiveness of photocatalytic dye degradation is largely dependent on the pH of the solution, as it affects both the surface charge of the photocatalyst and the ionization state of the dye molecules. The point of zero charge (pHpzc) of the Cu:ZnO/TiO_2 photocatalyst was determined to be around 6.8, indicating that the surface becomes positively charged at pH < pHpzc and negatively charged at pH > pHpzc [63]. Fig. 15 a and b showed that the photodegradation of turquoise blue (TBG) dye was examined at different pH levels: 4, 7, and 10. The results revealed a significant variation in degradation efficiency with changes in pH. At an acidic pH of 4, the photocatalytic process exhibited the highest degradation efficiency, achieving a removal rate of 94.61% and COD removal was 77.78%. The photocatalyst's enhanced performance is a result of electrostatic attraction. The positively charged surface of the catalyst attracts the negatively charged (anionic) dye molecules. This attraction increases the adsorption of the dye onto the catalyst, which in turn leads to greater photocatalytic activity. At neutral and basic pH (7 and 10), the catalyst surface becomes less positively charged or even negatively charged (above pHpzc), resulting in electrostatic repulsion with anionic TBG molecules. Consequently, fewer dye molecules are adsorbed on the active sites, lowering the overall degradation efficiency to 89.84% and 80.7%, respectively. TBG dye is anionic dye therefore, the interaction of negatively charged dyes with a positively charged photocatalyst catalytic surface promotes adsorption in acidic environments [58]. Kinetic analysis revealed that the photocatalytic degradation followed pseudo-first-order kinetics according to the equ. (12). The apparent rate constant (k_{app}) was found to be 1.1206 h^{-1} (0.019 min^{-1}), 0.911 h^{-1} (0.0152 min^{-1}), and 0.7612 h^{-1} (0.0123 min^{-1}) for pH 4, 7, and 10, respectively shown in Fig. 15 (c), confirming that the degradation rate decreases with increasing pH. The higher rate constant at pH 4 corresponds well with the improved surface adsorption and efficient charge separation at acidic conditions.

Furthermore, Fig. 16 showed COD of degraded sample at 4, 7 and 10 pH. Highest 77.78% COD degradation observed at pH 4. With pH 4, being the ideal value under the investigated conditions, these results imply that acidic conditions are more conducive to the photocatalytic breakdown of turquoise blue dye.

3.11. Recyclability study of synthesized photocatalyst

To assess the stability and reusability of the 7% Cu: ZnO/TiO_2 heterojunction photocatalyst for the degradation of TBG dye under UV light irradiation, a recyclability study was carried out. The photocatalyst was subjected to repeated degradation cycles, with each cycle involving 2.5 hours of UV irradiation in the presence of the dye solution. After each cycle, the catalyst was recovered by centrifugation, washed thoroughly with distilled water by magnetic stirrer, and dried at 100 oC for 1 h, and then calcined at 250 °C for 1 h. The catalyst was lightly calcined at 250 °C after each cycle to remove surface adsorbed organic residues without inducing any structural or compositional changes. Fig. 17 (a) and (b) illustrate the photocatalytic performance and stability of the 7% Cu:ZnO/TiO_2 nanophotocatalyst during TBG dye degradation under UV–visible irradiation. Fig. 17 (a) the plot of C/C_0 versus time shows the gradual decrease in dye concentration, while Fig. 17 (b) presents the corresponding photodegradation efficiency, which reached 84.3% after 2.5 h of irradiation. Additionally, Fig. 18 showed 60% COD degradation observed from the initial COD of the TBG dye sample. This sustained performance suggests that the synergistic effect between ZnO and TiO_2 not only enhances photocatalytic activity but also contributes to structural robustness and resistance to photo corrosion during prolonged UV exposure. These findings highlight the potential of 7% Cu: ZnO/TiO_2 as a durable photocatalyst for wastewater treatment applications involving persistent dye pollutants such as TBG dye.

4. Conclusion

A novel heterojunction photocatalyst, Cu: ZnO/TiO_2 (with copper doping concentrations varying from 3 wt% to 9 wt%), along with ZnO/TiO_2 heterojunction, pure TiO_2, and pure ZnO, was synthesized using a cost-effective sol-gel technique. All photocatalysts, both pure and heterojunction, were synthesized under ambient conditions and subsequently calcined at 500 °C for 2 hours. The optical, structural, morphological, surface chemical information, and chemical bonding characteristics of the prepared photocatalysts were analyzed using UV-Vis spectroscopy, XRD, FE-SEM, XPS, and FTIR, respectively. Both pure and heterojunction photocatalysts exhibited crystalline phases, and the formation of nanocrystals was confirmed by XRD analysis. FE-SEM revealed that the photocatalysts have a high surface area favorable for dye adsorption, thereby enhancing the photodegradation process. EDS mapping confirmed the presence of all constituent elements (Ti, Zn, Cu, and O) in appropriate proportions within the 7% Cu: ZnO/TiO_2. Optical studies showed that the 7% Cu: ZnO/TiO_2 photocatalyst achieved the most significant band gap reduction (3.0 eV) compared to pure TiO_2 (3.19 eV). The reduction in band gap, confirmed by a red shift, enhances photocatalytic activity by enabling greater absorption of visible light from the solar spectrum. The photocatalytic performance of all synthesized heterojunction photocatalysts was

evaluated by the degradation of Turquoise Blue G (TBG) dye in a photocatalytic reactor under UV light. The highest degradation efficiency, 95%, was achieved by the 7% Cu: ZnO/TiO_2 photocatalyst, which exhibited significantly improved photocatalytic activity compared to ZnO/TiO_2 and pure TiO_2. Additionally, the chemical oxygen demand (COD) of the treated wastewater was assessed using all synthesized photocatalysts. The 7% Cu: ZnO/TiO_2 catalyst showed the highest COD reduction efficiency, achieving a 77.78% decrease from the initial COD of TBG-containing wastewater. The effect of initial pH on the photocatalytic degradation of the anionic dye (TBG) under UV light in the presence of 7% Cu: ZnO/TiO_2 was also examined. Results indicated that the dye's adsorption capacity was highest at lower pH values, particularly at pH 4. Furthermore, the recyclability of the synthesized 7% Cu: ZnO/TiO_2 photocatalyst was investigated. Upon reuse, the recycled 7% Cu: ZnO/TiO_2 maintained a high photodegradation efficiency of 84.3%, demonstrating excellent photostability and recyclability.

Acknowledgements
The authors acknowledge the Sophisticated Analytical Instrument Facility (SAIF), Indian Institute of Technology (IIT), Bombay, Mumbai, X-Ray Lab, Department of MEMS, Indian Institute of Technology (IIT), Bombay, Mumbai, Maharashtra, India, for rendering analytical services for this work.

Authors contributions
Authors have contributed equally in preparing and writing the manuscript.

Availability of data and materials
The data that support the findings of this study are available from the corresponding author, upon reasonable request.

Conflict of interest
The authors declare no conflict of interest.

Funding
This research did not receive any specific grant from funding agencies in the public, commercial, or not-for-profit sectors.

References

[1] T.A. Khattab, M.S. Abdelrahman, and M. Rehan. *Environ. Sci. Pollut. Res.*, **27** (2020) 3803–3818. https://doi.org/10.1007/s11356-019-07137-z

[2] D. Chen, Y. Cheng, N. Zhou, P. Chen, Y. Wang, K. Li, S. Huo, P. Cheng, P. Peng, R. Zhang, L. Wang, H. Liu, Y. Liu, and R. Ruan. *J. Clean. Prod.,* **268** (2020)121725. https://doi.org/10.1016/j.jclepro.2020.121725

[3] K. S. Varma, R. J. Tayade, K. J. Shah, P. A. Joshi, A. D. Shukla, and V. G. Gandhi. *Water-Energy Nexus,* **3** (2020) 46–61. https://doi.org/10.1016/j.wen.2020.03.008

[4] A. I. Saber, K. Sharma, S. Aggarwal, A. Babbar, R. Kumar, A. Kaur, R. Badru, and S. Kaushal. *Emergent Mater,* **7** (2024) 1019–1030. https://doi.org/10.1007/s42247-024-00644-x

[5] D. Jalandhara, S. Kumar, J. Dalal, N. Supreet, G. Singh, S. Kumar, R. Badru, Y. Singh, S.V. Sharma, and S. Kaushal. *Mater. Adv.*, **6** (2024) 641–657. https://doi.org/10.1039/d4ma01053a

[6] J. Abdi, M. Yahyanezhad, S. Sakhaie, M. Vossoughi, and I. Alemzadeh. *J. Environ. Chem. Eng.,* **7** (2019) 103096. https://doi.org/10.1016/j.jece.2019.103096

[7] S. A. Mirsalari, A. Nezamzadeh-Ejhieh, and A. R. Massah. *Environ. Sci. Pollut. Res.*, **29** (2022) 33013–33032. https://doi.org/10.1007/s11356-021-17569-1

[8] M. R. D. Khaki, M. S. Shafeeyan, A. A. A. Raman, and W. M. A. W. Daud. *J. Environ. Manage.,* **198** (2017) 78–94. https://doi.org/10.1016/j.jenvman.2017.04.099

[9] J. Gaur, S. Kumar, M. Pal, H. Kaur, Supreet, R. Badru, J. Momoh, R. Pal, and S. Kumar. *Adv. Nat. Sci.: Nanosci. Nanotechnol.,* **14** (2023) 035014. https://doi.org/10.1088/2043-6262/acf28a

[10] A. M. Sescu, L. Favier, D. Lutic, N. Soto-Donoso, G. Ciobanu, and M. Harja. *Water*, **13** (2021) 19. https://doi.org/10.3390/w13010019

[11] M. Lanjewar, and J. V. Gohel. *Inorg. Nano-Met. Chem.,* **47** (2017) 1090–1096. https://doi.org/10.1080/24701556.2016.1241275

[12] M. Lanjewar, and J. V. Gohel. *Bull. Mater. Sci.,* **41** (2018) 1–7. https://doi.org/10.1007/s12034-018-1664-5

[13] C. M. Pelicano, and H. Yanagi. *J. Mater. Chem. C Mater,* **7** (2019) 4653–4661. https://doi.org/10.1039/c9tc00401g

[14] K. C. Hsu, T. H. Fang, Y. J. Hsiao, and P. C. Wu. *J. Alloys Compd.,* **794** (2019) 576–584. https://doi.org/10.1016/j.jallcom.2019.04.238

[15] H. M. Mousa, J. F. Alenezi, I. M. A. Mohamed, A. S. Yasin, A. F. M. Hashem, and A. Abdal-hay. *J. Alloys. Compd.,* **886** (2021) 161169. https://doi.org/10.1016/j.jallcom.2021.161169

[16] R. G. Nair, A. Das, S. Paul, B. Rajbongshi, and S.K. Samdarshi. *J. Alloys. Compd.,* **695** (2017) 3511–3516. https://doi.org/10.1016/j.jallcom.2016.12.002

[17] W. Feng, L. Lin, H. Li, B. Chi, J. Pu, and J. Li. *Int. J. Hydrogen Energy,* **42** (2017) 3938–3946. https://doi.org/10.1016/j.ijhydene.2016.10.087

[18] X. He, T. Kai, and P. Ding. *Environ. Chem. Lett.*, **19** (2021) 4563-1601. https://doi.org/10.1007/s10311-021-01295-8

[19] K. Afroz, M. Moniruddin, N. Bakranov, S. Kudaibergenov, and N. Nuraje. *J. Mater. Chem. A Mater.,* **6** (2018) 21696–21718. https://doi.org/10.1039/c8ta04165b

[20] M. Mersal, A. F. Zedan, G. G. Mohamed, and G. K. Hassan. *Sci. Rep.,* **13** (2023) 1–15. https://doi.org/10.1038/s41598-023-31625-5

[21] M. R. Al-Mamun, S. Kader, M.S. Islam, and M.Z.H. Khan. *J. Environ. Chem. Eng.,* **7** (2019) 103248. https://doi.org/10.1016/j.jece.2019.103248

[22] P. Bharathi, S. Harish, J. Archana, M. Navaneethan, S. Ponnusamy, C. Muthamizhchelvan, M. Shimomura, and Y. Hayakawa. *Appl. Surf. Sci.,* **484** (2019) 884–891. https://doi.org/10.1016/j.apsusc.2019.03.131

[23] A. El Mragui, I. Daou, and O. Zegaoui. *Catal. Today.,* **321–322** (2019) 41–51. https://doi.org/10.1016/j.cattod.2018.01.016

[24] A. Prabhu, P. C. Meenu, and S. Roy. *New J. Chem.,* **48** (2024) 10552–10562. https://doi.org/10.1039/d4nj00407h.

[25] Y. Liao, P. Deng, X. Wang, D. Zhang, F. Li, Q. Yang, H. Zhang, and Z. Zhong. *Nanoscale Res. Lett.,* **13** (2018) 221. https://doi.org/10.1186/s11671-018-2637-8

[26] R. Kumar, R. M. El-Shishtawy, and M.A. Barakat. *Catalysts*, **6** (2016) 76. https://doi.org/10.3390/catal6060076

[27] A. M. A. Noman, M. A. Alghobar, and S. Suresha. *J. Water Environ. Nanotechnol.,* **6** (2021) 1–10. https://doi.org/10.22090/jwent.2021.01.001

[28] C. B. D. Marien, C. Marchal, A. Koch, D. Robert, and P. Drogui. *Environ. Sci. Pollut. Res.,* **24** (2017) 12582–12588. https://doi.org/10.1007/s11356-016-7681-2

[29] W. Bahnemann, V. K. Landge, C. M. Huang, V. S. Hakke, S. H. Sonawane, S. Manickam, and M. C. Hsieh. *Catalysts*, **12** (2022) 605. https://doi.org/10.3390/catal

[30] A. Gunasekaran, A. K. Rajamani, C. Masilamani, I. Chinnappan, U. Ramamoorthy, and K. Kaviyarasu. *Catalysts,* **13** (2023) 215. https://doi.org/10.3390/catal13020215

[31] A. Phuruangrat, Y. Chimupala, A. Somdee, B. Kuntalue, T. Thongtem, and S. Thongtem. *Iran. J. Catal.,* **15** (2025) 152526–152527. https://doi.org/10.57647/j.ijc.2025.1503.26

[32] M. Rezaei, A. A. Ensafi, and E. Heydari-Bafrooei. *J. Ind. Eng. Chem.,* **146** (2025) 589–602. https://doi.org/10.1016/j.jiec.2024.11.043

[33] N. Mintcheva, S. Yamaguchi, and S. A. Kulinich. *Materials*, **13** (2020) 719. https://doi.org/10.3390/ma13030719

[34] W. Navarra, I. Ritacco, O. Sacco, L. Caporaso, M. Farnesi Camellone, V. Venditto, and V. Vaiano. *J. Phys. Chem. C,* **126** (2022) 7000–7011. https://doi.org/10.1021/acs.jpcc.2c00152

[35] S. Khammarnia, and H. Hassani. *Iran. J. Catal.,* **15** (2025) 152514–152515. https://doi.org/10.57647/j.ijc.2025.1502.14

[36] N. M. Alatawi, L. Ben Saad, L. Soltane, A. Moulahi, I. Mjejri, and F. Sediri. *Polyhedron*, **197** (2021) 115022. https://doi.org/10.1016/j.poly.2021.115022

[37] I. Aadnan, O. Zegaoui, A. El Mragui, H. Moussout, J.C.G. and Esteves da Silva. *Arab. J. Chem.,* **17** (2024) 105336. https://doi.org/10.1016/j.arabjc.2023.105336

[38] I. Ben Elkamel, N. Hamdaoui, A. Mezni, R. Ajjel, and L. Beji. *J. Mater. Sci.: Mater. Electron.,* **30** (2019) 9444–9454. https://doi.org/10.1007/s10854-019-01276-2

[39] B. A. Lemecho, F. K. Sabir, D. M. Andoshe, N. S. Gultom, D. H. Kuo, X. Chen, E. Mulugeta, T. D. Desissa, O. and A. Zelekew. *Bioinorg. Chem. Appl.,* **2022** (2022) 1-10. https://doi.org/10.1155/2022/8081494

[40] R. Ahmadiasl, G. Moussavi, S. Shekoohiyan, and F. Razavian. *Catalysts*, **12** (2022) 1310. https://doi.org/10.3390/catal12111310

[41] M. Al-Amin, S. Chandra Dey, T.U. Rashid, M. Ashaduzzaman, and S.M. Shamsuddin. *Int. J. Latest Res. Eng. Technol.,* **2** (2016) 14–21.

[42] A. Putta, and J. V. Vastrad. *J. Eco-Friendly Agric.,* **18** (2023) 37–42. https://doi.org/10.5958/2582-2683.2023.00007.2

[43] D. Kumbhar, S. Kumbhar, S. Delekar, R. Nalawade, and A. Nalawade. *Nanosyst.: Phys. Chem. Math.* **10** (2019) 466–474. https://doi.org/10.17586/2220-8054-2019-10-4-466-474

[44] J. Li, L. Yan, Y. Wang, Y. Kang, and C. Wang. *J. Mater. Sci.: Mater. Electron.*, **27** (2016) 7834–7838. https://doi.org/10.1007/s10854-016-4773-1

[45] Y. Sun, Y. Gao, B. Zhao, S. Xu, C. Luo, and Q. Zhao. *Mater. Res. Express,* **7** (2020) 085010. https://doi.org/10.1088/2053-1591/abaea4

[46] Y. Zhang, X. Bo, T. Zhu, W. Zhao, Y. Cui, and J. Chang. *Nanomaterials*, **14** (2024) 1802. https://doi.org/10.3390/nano14221802

[47] O. Mbrouk, H. Hafez, S. Mozia, A. M. Othman, and M. S. A. Abdel Mottaleb. *BMC Chem.*, **16** (2022) 74. https://doi.org/10.1186/s13065-022-00866-2

[48] Y. Tai, B. Yang, J. Li, L. Meng, P. Xing, and S. Wang. *Molecules*, **29** (2024) 5028. https://doi.org/10.3390/molecules29215028

[49] M. Rezaei, A. Nezamzadeh-Ejhieh, and A. R. Massah. *Energy and Fuels,* **38** (2024) 8406–8436. https://doi.org/10.1021/acs.energyfuels.4c00160

[50] G. Issa, S. Kříženecká, P. Bezdička, D. Popelková, M. Kormunda, J. Ederer, D. Bůžek, J. Čundrle, Z. Baďura, J. Henych, and M. Šťastný. *Catal. Sci. Technol.,* **15** (2025) 4438–4456. https://doi.org/10.1039/d4cy01400f

[51] J. Khumphon, R. Ahmed, T. Imboon, J. Giri, N. Chattham, F. Mohammad, S. Kityakarn, V. Mangala Gowri, and S. Thongmee. *ACS Omega,* **10** (2025) 9337–9350. https://doi.org/10.1021/acsomega.4c10034

[52] M. Rezaei, and A. Nezamzadeh-Ejhieha. *Int. J. Hydrogen Energy,* **45** (2020) 24749–24764. https://doi.org/10.1016/j.ijhydene.2020.06.258

[53] M. Rezaei, A. Nezamzadeh-Ejhieh, and A. R. Massah. *ACS Omega*, **9** (2024) 6093–6127. https://doi.org/10.1021/acsomega.3c07560

[54] A. Kumar, P. Choudhary, A. Kumar, P. H. C. Camargo, and V. Krishnan. *Small*, **18** (2022) 2101638. https://doi.org/10.1002/smll.202101638

[55] M. Rezaei, A. Nezamzadeh-Ejhieh, and A. R. Massah. *Energy and Fuels*, **38** (2024) 7637–7664. https://doi.org/10.1021/acs.energyfuels.4c00325

[56] P. Balla, P. K. Seelam, R. Balaga, R. Rajesh, V. Perupogu, and T. X. Liang. *J. Environ. Chem. Eng.,* **9** (2021) 106530. https://doi.org/10.1016/j.jece.2021.106530

[57] H. Derikvandi, M. Vosough, and A. Nezamzadeh-Ejhieh. *Environ. Sci. Pollut. Res.,* **27** (2020) 27582–27597. https://doi.org/10.1007/s11356-020-08817-x

[58] S. Das, and H. Mahalingam. *J. Environ. Chem. Eng.,* **7** (2019) 103289. https://doi.org/10.1016/j.jece.2019.103289

[59] S. Sakarkar, S. Muthukumran, and V. Jegatheesan. *J. Environ. Manage.,* **272** (2020) 111090. https://doi.org/10.1016/j.jenvman.2020.111090

[60] S. Noreen, S. Zafar, I. Bibi, M. Amami, M. A. S. Raza, F. H. Alshammari, Z.M. Elqahtani, B. I. Basha, N. Alwadai, A. Nazir, M. I. Khan, and M. Iqbal. *Ceram. Int.,* **48** (2022) 12170–12183. https://doi.org/10.1016/j.ceramint.2022.01.078

[61] N. W. Putra, I. W. B. Suyasa, I. W. Suarna, A. A. S. A. Sukmaningsih, and I. D. K. Sastrawidana. *Ecol. Eng. Environ. Technol.,* **26** (2025) 233–244. https://doi.org/10.12912/27197050/200189

[62] A. I. Alwared, N. A. Mohammed, T. J. Al-Musawi, and A. A. Mohammed. *Sustainability,* **15** (2023) 10815. https://doi.org/10.3390/su151410815

[63] H. D. Tran, D. Q. Nguyen, P. T. Do, and U. N. P. Tran. *RSC Advances,***13** (2023) 16915–16925. https://doi.org/10.1039/d3ra01970e

[64] S. Sharafzadeh, J. Zolgharnein, A. Nezamzadeh–Ejhieh, and S. D. Farahani. *Int. J. Hydrogen Energy,* **106** (2025) 1429–1442. https://doi.org/10.1016/j.ijhydene.2025.02